Multiresolution Imaging in Elastography

Tomy Varghese, *Member, IEEE*, Mehmet Bilgen, *Member, IEEE*, and Jonathan Ophir, *Member, IEEE*

***Abstract*—The range of strains that can be imaged by any practical elastographic imaging system is inherently limited, and a performance measure is valuable to evaluate these systems from the signal and noise properties of their output images. Such a measure was previously formulated for systems employing cross-correlation based time-delay estimators through the strain filter. While the strain filter predicts the signal-to-noise ratio (SNR_e) for each tissue strain in the elastogram and provides valuable insights into the nature of image noise, it understated the effects of image resolution (axial resolution, as determined by the cross-correlation window length) on the noise. In this work, the strain filter is modified to study the strain noise at multiple resolutions. The effects of finite window length on signal decorrelation and on the variance of the strain estimator are investigated. Long-duration windows are preferred for improved sensitivity, dynamic range, and SNR_e. However, in this limit the elastogram is degraded due to poor resolution. The results indicate that for nonzero strain, a window length exists at which the variance of strain estimator attains its minima, and consequently the elastographic sensitivity, dynamic range and SNR_e are strongly affected by the selected window length. Simulation results corroborate the theoretical results, illustrating the presence of a window length where the strain estimation variance is minimized for a given strain value.**

Multiresolution elastography, where the strain estimate with the highest SNR_e obtained by processing the pre- and post-compression waveforms at different window lengths is used to generate a composite elastogram and is proposed to improve elastograms. All the objective elastogram parameters (namely: SNR_e, dynamic range, sensitivity and the average elastographic resolution—defined as the cross-correlation window length) are improved with multiresolution elastography when compared to the traditional method of utilizing a single window length to generate the elastogram. Experimental results using a phantom with a hard inclusion illustrates the improvement in elastogram obtained using multiresolution analysis.

I. Introduction

Elastography is a method for imaging the elastic properties of biological tissues in vivo, and elastograms are gray scale images that depict the distribution of strains in tissue [1]–[3]. The elastograms are formed by a process involving two steps (Fig. 1). First, the tissue is compressed externally to generate an internal strain field. Second, ultrasonic echo signals before and after compression are acquired and processed. The elastic modulus distribution and the boundary conditions determine the actual strain distribution in the compressed tissue. The strain distribution is estimated from the pre- and post-compression echo signals. These signals are segmented at different depths by partially overlapping windows, and the waveforms in each window are cross-correlated to estimate the time-delays. Next, two time delay estimates from the overlapping windows are used to estimate the axial strain field. The amount of overlap between the windows and the window length are the two parameters that are related to the resolution in elastograms. If the overlap factor is fixed as a fraction of the window length, the window length can be defined as an effective resolution parameter. The estimation performance of the strain estimator in response to a strain step also results in a linear transition zone between the two strain levels that corresponds to the window length, thereby relating the window length to the axial resolution parameter [3]. Small windows with fixed overlap produce high resolution but noisy elastograms.

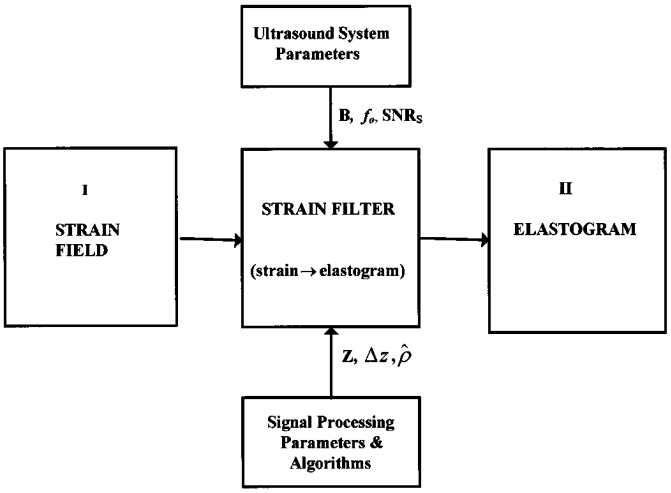

Fig. 1. The block diagram of the strain filter, indicating the filtering of the tissue strains by the strain filter allowing the prediction of the elastogram parameters. The process of generating an elastogram can be viewed as a two-step process: first, tissue is compressed to obtain a strain field, and second, ultrasonic echo correlation techniques are used to estimate the axial strain field. The contributions of the signal processing and ultrasound system parameters are indicated as inputs into the strain filter. Improvements in estimator performance due to other algorithms are introduced through enhancements in the correlation coefficient.

The range of actual strains that can be imaged varies greatly with the elastographic imaging system, while the statistical properties of the strain estimate depends on many parameters, including the actual strain and the resolution. To evaluate the performance of these systems, an

Manuscript received September 23, 1996; accepted July 29, 1997. This work was supported in part by NIH grants R01-CA38515, R01-CA60520, and P01-CA64579, and by a grant from Diasonics Corp., Santa Clara, CA.

T. Varghese and J. Ophir are with the Ultrasonics Laboratory, Department of Radiology, The University of Texas Medical School, Houston, TX 77030 (e-mail: tomyv@msrad3.med.uth.tmc.edu).

M. Bilgen is with the Department of Radiology, University of Kansas Medical Center, Kansas City, KS 66160-7234.

objective criterion is required to assess the accuracy and precision of the strain estimates. One such criterion that quantitatively measures the accuracy and precision of the strain estimates is the elastographic signal-to-noise ratio (SNR_e) [4] defined by:

$$\mathrm{SNR}_e = \frac{m_s}{\sigma_s}. \tag{1}$$

Here m_s denotes the statistical mean strain estimate and σ_s denotes the standard deviation for the strain noise estimated from the elastogram. The variation of the SNR_e with tissue strain gives the strain transfer function of the elastographic system. When the statistical mean value of the strain is replaced by the ideal tissue strain, and the minimum standard deviation by the theoretical lower bound on the standard deviation, we obtain an upper bound on the performance of the strain estimator, referred to as the strain filter [4]. The strain filter therefore represents a theoretical upper bound on the transfer function of an elastographic imaging system that defines the mapping from the entire range of strains present in the compressed tissue via the first order statistical properties of the elastogram. The upper bound may be derated to account for other noise sources such as digitization noise, tissue attenuation [5], and lateral and elevational decorrelation [6].

The strain filter depends on the correlation coefficient between the windowed signal waveforms [4]. An expression derived previously for the strain filter [4] was for large windows to evaluate low-resolution elastograms. In this paper, we derive the correlation coefficient and strain filter for finite window lengths. The result is called the multiresolution strain filter. This new formalism effectively combines the ultrasound system parameters [center frequency, bandwidth, and sonographic signal-to-noise ratio (SNR_S)] with the particulars of the signal processing algorithms (namely, the window length and the overlap factor). The range of strains in the elastogram and their respective elastographic SNR_e, therefore, can be measured at different resolutions.

The strain filter shows that the measurement process allows only a selected range of strains to be displayed on the elastogram, and consequently has bandpass characteristics in the strain domain. The width and the height of the strain filter specifies the dynamic range (DR_e) and SNR_e of the elastographic imaging system as defined in the Appendix. The strain filter has previously been used to analyze the tradeoffs in the strain estimation performance for different ultrasound system parameters; namely, the bandwidth and center frequency [4], algorithms like multicompression [7], [8], temporal stretching [8], and extension of the dynamic range in the elastogram [9]. The dynamic range extension algorithm uses variable applied compression along with a careful selection of the strains in the corresponding elastograms with the highest SNR_e to generate the composite elastogram [9]. The strain filter formalism was also used recently to evaluate the tradeoffs in the use of RF and envelope signals for strain estimation [10]. The nonstationary variation of the strain filter with frequency dependent attenuation [5] and lateral and elevational signal decorrelation [6] also have been analyzed.

In this paper, we investigate the effects of parameters regarding the ultrasonic system and the signal processing algorithm on the dynamic range and the sensitivity of the multiresolution strain filter. Elastographic images generated from experimental data and numerical simulations for a variety of resolution conditions are compared with the predictions of the multiresolution strain filter.

The paper is organized as follows. Additional description of the strain filter formalism is presented in Section II. In Section III, an expression for the correlation coefficient that depends on the window length is derived. Section IV describes the theory for the computation of the axial strain variance and the development of the multiresolution strain filter. Simulation results in Section V verify the presence of a window length where the strain estimation variance is minimized, as predicted by the theoretical analysis. Experimental results in Section VI illustrate the application of multiresolution elastography to improve the elastogram parameters. The bias errors observed by Céspedes [3] also are reduced with multiresolution elastography. Section VII discusses and summarizes the paper.

II. Background

Axial strain ($\hat{s}$) is estimated from ultrasonic echo signals segmented by two adjacent windows [1]:

$$\hat{s} = \frac{\hat{d}_2 - \hat{d}_1}{\Delta z}, \tag{2}$$

where $\hat{d}_1$ is the displacement estimate from the window centered at location z, Δz is the window separation determining the overlap factor, and $\hat{d}_2$ is the displacement estimate from the window at location $z + \Delta z$.[1] Because the strain estimate is obtained from a linear combination of two random variables, $\hat{d}_1$ and $\hat{d}_2$, the variance of the strain estimator depends on the variances of these variables. Assuming that the echo signals are stationary, the variance of the strain estimate ($\sigma^2_{\hat{s}}$) can be expressed in terms of the variance of the displacement (time-delay) estimates ($\sigma^2_{\hat{d}}$) [11]:

$$\sigma^2_{\hat{s}} \geq \frac{2\sigma^2_{\hat{d}}}{Z\Delta z} \tag{3}$$

where Z denotes the window length. From the inequality in (3), it appears that the strain estimation variance can be reduced monotonically by increasing the window length Z or window separation Δz.

The variation in the upper bound of the elastographic SNR_e with tissue strain is defined as the strain filter, and is given by:

$$\mathrm{SNR}_e^{\mathrm{UB}} = \frac{s_t}{\sigma(\hat{s})_{\mathrm{ZZLB},\rho}}, \tag{4}$$

[1]Note that time delay estimates and displacement estimates are often used interchangeably by assuming that the speed of sound in the tissue is constant.

where s_t is the tissue strain, and $\sigma(\hat{s})_{\mathrm{ZZLB},\rho}{}^2$ is the modified Ziv-Zakai lower bound (ZZLB) [12] on the standard deviation of the strain estimator. The ZZLB provides the tightest lower bound for the displacement estimator. The modified ZZLB expression for the strain estimation variance [4] is given by:

$$\sigma^2(\hat{s})_{\mathrm{ZZLB},\rho} \geq \begin{cases} \frac{(sZ)^2}{6Z\Delta z}, & (2BZ/c)\mathrm{SNR}_C < \gamma \\ \text{Threshold} & \gamma < (2BZ/c)\mathrm{SNR}_C < \delta \\ \sigma^2(\hat{s})_{\mathrm{BB},\rho} = \frac{2\sigma^2(\hat{d})_{\mathrm{BB},\rho}}{Z\Delta z} & \delta < (2BZ/c)\mathrm{SNR}_C < \vartheta \\ \text{Threshold} & \vartheta < (2BZ/c)\mathrm{SNR}_C < \eta \\ \sigma^2(\hat{s})_{\mathrm{CRLB},\rho} = \frac{2\sigma^2(\hat{d})_{\mathrm{CRLB},\rho}}{Z\Delta z} & \eta < (2BZ/c)\mathrm{SNR}_C \end{cases} \quad (5)$$

where Z is the length of the temporal window, SNR_C denotes the composite signal-to-noise ratio in the RF signal (defined in Appendix A), $\sigma^2(\cdot)_{\mathrm{CRLB},\rho}$ represents the Cramér-Rao lower bound (CRLB) on the variance, for partially correlated signals with nonzero strain [13], and $\sigma^2(\cdot)_{\mathrm{BB},\rho}$ represents the corresponding Barankin bound. The Barankin bound exceeds CRLB by a factor of $12(f_0/B)^2$ [12]. For zero strain $\sigma^2(\hat{d})_{\mathrm{CRLB},\rho}$ converges to the classical CRLB where $\sigma^2(\hat{d})_{\mathrm{CRLB}} \propto Z^{-1}$ for large windows [12]–[15]. The quantity $(2BZ/c)\mathrm{SNR}_C$ is referred to as the postintegration SNR. Equation (5) shows the three distinct operating regions for $\sigma^2(\hat{s})_{\mathrm{ZZLB},\rho}$ depending on the value of in [12], and in the Appendix B.

For partially correlated signals within the window, Walker and Trahey [13] derived a minimum variance for the displacement estimator that depends on the correlation coefficient. The assumption that the waveforms have a rectangular spectrum led to the following closed-form expression:

$$\sigma^2(\hat{s})_{\mathrm{CRLB},\rho} \cong \frac{3c}{4\pi^2 Z(B^3 + 12Bf_0^2)} \left[\frac{1}{\rho^2} \left(1 + \frac{1}{\mathrm{SNR}_S^2} \right)^2 - 1 \right] \quad (6)$$

where the term SNR_S represents the signal-to-noise ratio due to the signal independent noise in echo signals. The parameter ρ denotes the correlation coefficient and accounts for the effects of partial correlation of the waveforms within the window. For zero strain $\rho = 1$, (6) reduces to the classical expressions for the CRLB [12]–[15]. For non-zero strain $\rho < 1$, (6) increases the bound to a more achievable level $\sigma^2(\hat{d})_{\mathrm{CRLB},\rho} > \sigma^2(\hat{d})_{\mathrm{CRLB}}$. Furthermore, we will show in Section IV that the strain estimation variance is minimum for a characteristic window length (Z) for each strain, and beyond which $\sigma^2(\hat{s})_{\mathrm{CRLB},\rho}$ increases rapidly with Z. The minimum variance for the strain estimator is obtained by substituting (6) into (5). Previous work [17] suggests that a 50% window overlap provides the best strain estimates. With $\Delta z = Z/2$, the window length Z is the only parameter left defining the resolution in elastograms. The smallest Z that can be selected in processing the echo waveforms would be the duration of the impulse response (determined by the bandwidth and the center frequency) of the ultrasound system. The best resolution in elastograms is, therefore, limited by the duration of the system impulse response.

An expression for ρ was previously derived by Walker and Trahey [16] for point scatterers illuminated by an ultrasonic transducer with rectangular spectrum. In the next section, we derive the correlation coefficient ρ for correlated scatterers illuminated by broadband transducers that also include the effects of tissue strain and finite duration windows.

III. Formulation of the Correlation Coefficient

The following expression for the correlation coefficient is based on the treatment of Bilgen and Insana [18]. However, the expression of the correlation coefficient presented in this paper includes the contributions arising from the use of a finite cross-correlation window. First the ultrasonic RF echo signals are modeled by:

$$\begin{aligned} r_1(z) &= h(z) * e(z) + n_1(z), \\ r_2(z) &= h(z) * e(az) + n_2(z) \end{aligned} \quad (7)$$

where the subscripts $_1$ and $_2$, respectively, specify the pre- and post-compression echo-signals obtained from an elastic tissue medium, $e(z)$ is the scattering function of the tissue, $h(z)$ is the pulse-echo point-spread function (PSF) of the imaging system, and $n_1(z)$ and $n_2(z)$ are the uncorrelated, zero mean random noise. The symbol $*$ denotes the convolution operation. The parameter a compressing the tissue scattering function is the strain factor defined in terms of either the actual tissue strain s, $a = 1/(1-s) \sim 1+s$ for $s \ll 1$ or the residual strain δs, $a \sim 1 + \delta s$ if the post-compression echo signal is stretched back temporally by the average strain. In either case, a is not constant and changes continuously with position in the tissue. However, (7) treats the strain as locally constant within each window because any continuous profile can be approximated by a piece-wise variation. For varying strain within the window, only an average estimate of the strain is obtained. Hereafter we use the word strain to mean either s or δs and the word post-compression to mean either the signal received from tissue after the compression or the signal stretched back by the average strain.

The impulse response function h(z) is represented by a Gaussian modulated sinusoid as:

$$h(z) = \frac{1}{\sqrt{2\pi}L_h} \exp(-z^2/2L_h^2) \sin(k_0 z), \quad (8)$$

where k_0 is the spatial center frequency, and L_h is the duration of the ultrasound pulse. The tissue scattering function is realized from a filtered white noise process [19], [20]. The

[2]The lower bounds on the strain estimation variance are denoted with an additional subscript ρ to illustrate that these variance are computed for partially correlated signals. These lower bounds converge to the classical bounds when $\rho = 1$.

autocorrelation of the scattering function is represented by a Gaussian centered at a spatial frequency k_f:

$$e(z) = \frac{1}{\sqrt{2\pi}L_f} \exp(-z^2/2L_f^2) \cos(k_f z), \tag{9}$$

where L_f represents a correlation length representing the longitudinal variation in tissue. The amplitude spectrum of the filter function is given by:

$$E(k) = \frac{1}{2}(\exp(-(k+k_f)^2 L_f^2/2) + \exp(-(k-k_f)^2 L_f^2/2)). \tag{10}$$

With the echo signal model presented in (7) and the above assumptions, we first derive the cross-correlation function between the pre- and post-compression waveforms

$$\langle \hat{\Gamma}_{12}(z') \rangle = \left\langle \frac{1}{Z} \int_{-Z/2}^{Z/2} r_1(z-z') r_2(z)\, dz \right\rangle \tag{11}$$

and the correlation functions $\hat{\Gamma}_{11}(z)$ for the pre- and $\hat{\Gamma}_{22}(z')$ the post-compression waveforms. The square bracket $\langle \cdot \rangle$ denotes the ensemble average, and z' denotes the shift variable. The effective correlation coefficient can be written as:

$$\rho = \frac{\hat{\Gamma}_{12}(0)}{\sqrt{\hat{\Gamma}_{11}(0)\hat{\Gamma}_{22}(0)}} = \rho_0 \times M. \tag{12}$$

The term ρ_0 represents the peak correlation coefficient [18], and can be expressed as:

$$\rho_0 = \frac{(L_f^2 + L_h^2)^{1/4}(L_f^2 + a^2 L_h^2)^{1/4}}{\eta} \times \exp\left(\frac{\zeta^2}{\eta^2} - \frac{1}{2}\left(\frac{(\omega_f L_f^2 + \omega_0 L_h^2)^2}{L_f^2 + L_h^2} + \frac{(\omega_f L_f^2 + a\omega_0 L_h^2)^2}{L_f^2 + a^2 L_h^2} \right) \right) \tag{13}$$

where

$$\eta^2 = L_f^2 + \frac{1+a^2}{2} L_h^2$$
$$\zeta = \omega_f L_f^2 + \frac{1+a}{2} \omega_0 L_h^2.$$

The factor M in (12) is due to the finiteness of the window length and is given by the integral:

$$M = \frac{1}{Z} \int_{-Z/2}^{Z/2} \exp\left(-\frac{((1-a)z)^2}{4\eta^2} \right) \cos\left(\frac{\zeta((1-a)z)}{\eta^2} \right) dz. \tag{14}$$

Evaluating the integral yields:

$$M = \frac{\sqrt{\pi}\eta \exp\left(-\frac{\zeta^2}{\eta^2}\right)}{(1-a)Z} \left\{ \operatorname{erf}\left[\frac{(1-a)Z + i4\zeta}{4\eta} \right] - \operatorname{erf}\left[\frac{-(1-a)Z + i4\zeta}{4\eta} \right] \right\} \tag{15}$$

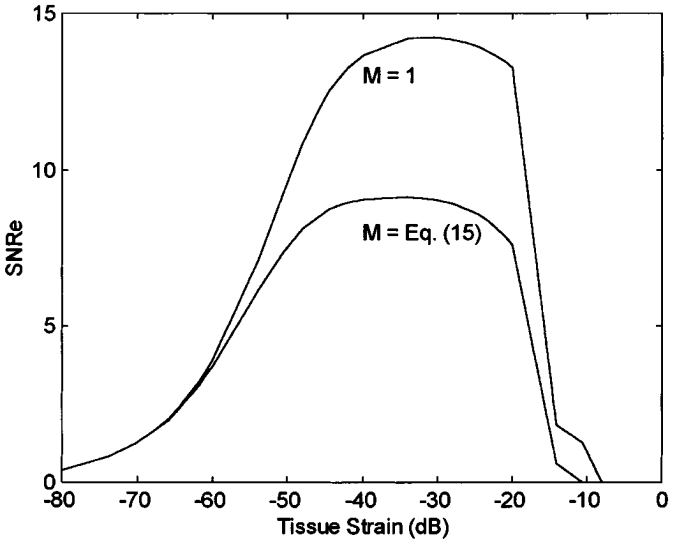

Fig. 2. Comparison of the strain filters obtained using the effective correlation coefficient as opposed to the peak correlation coefficient. The strain filters were obtained using the following parameters: $L_h = L_f = 0.1$ mm, $k_0 = k_f = 20.4$ mm^{-1}.

where $\operatorname{erf}(\cdot)$ is the error function defined as:

$$\operatorname{erf}(x) = \frac{2}{\sqrt{\pi}} \int_0^x \exp(-z^2)\, dz. \tag{16}$$

For zero strain $s = 0$, $a = 1$ and one can show that $M = 1$ in the limit. Nonzero strains on the other hand yield $M < 1$ and consequently reduces the correlation coefficient ρ. A comparison of the strain filters with the additional reduction in the correlation coefficient (since $M < 1$ for nonzero strain and finite window lengths) and previously published strain filters [4], for a 1 mm resolution is illustrated in Fig. 2. Tissue strain in decibels is plotted along the x-axes, where 0 dB corresponds to a 100% tissue strain. Note the reduction in the maximum value of the SNR_e and dynamic range due to the contributions of the factor M on the strain filter. The difference between the strain filter due to the effect of the additional decorrelation will be more pronounced with an increase in the window length.

IV. Theoretical Results

In this section, we use the correlation coefficient ρ in (12) and compute $\sigma^2(\hat{s})_{\mathrm{CRLB},\rho}$ in (6) to determine the lower bound on the strain variance $\sigma^2(\hat{s})_{\mathrm{ZZLB},\rho}$ in (5). Next we calculate the multiresolution strain filter from (4). We use the following parameter values for the calculations unless stated otherwise: $L_h = L_f = 0.1$ mm $k_0 = k_f = 20.4$ mm^{-1} (denoting an ultrasound pulse with a 5 MHz center frequency) and $\Delta z = Z/2$ (i.e., 50% window overlap between data segments).

The variation of correlation coefficient ρ in (12) with the window length Z is illustrated in Fig. 3, for five differ-

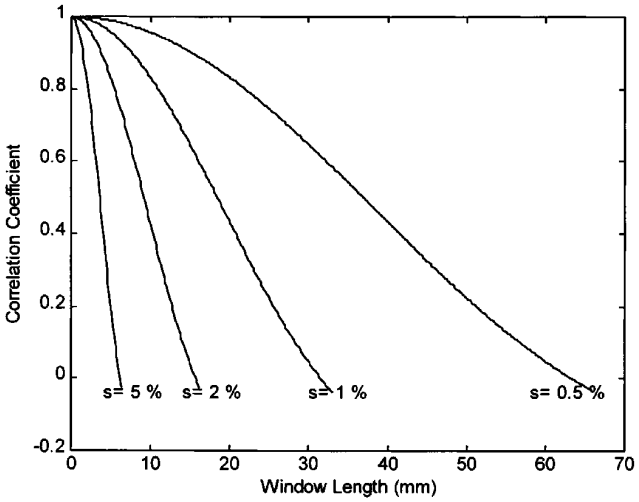

Fig. 3. Variation of the effective correlation coefficient for different strain values plotted as a function of the window length. Observe that the correlation coefficient decays rapidly with an increase in tissue strain. The effective correlation coefficients were obtained using the following parameters: $L_h = L_f = 0.1$ mm, $k_0 = k_f = 20.4$ mm^{-1}.

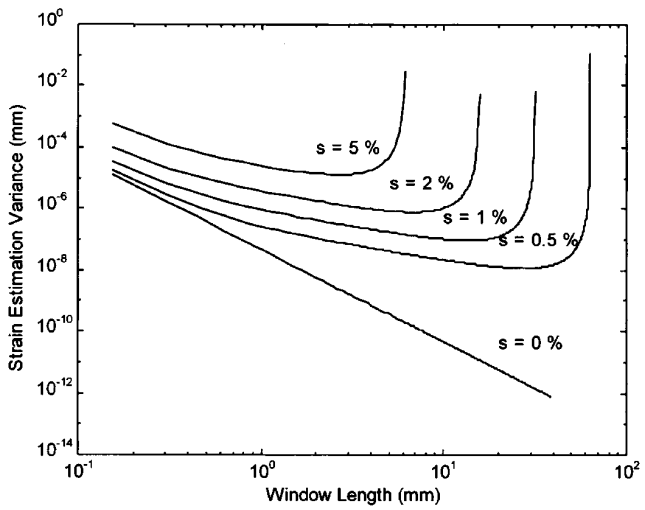

Fig. 4. Standard deviation of tissue strain estimates plotted as a function of the window length. Observe that, for the case of zero strain, where the variance reduces with an increase in the window length as predicted by CRLB theory. For all other values of the strain, we obtain an optimal window length where the standard deviation is minimum. The length of the optimum window reduces with an increase in tissue strain. The strain estimation variances were obtained using the following parameters: $L_h = L_f = 0.1$ mm, $k_0 = k_f = 20.4$ mm^{-1}.

ent strain values: $s = 0\%$, 0.5%, 1%, 2%, and 5%. For zero strain $s = 0$, $\rho = 1$ and for nonzero strain $s > 0$, $\rho \leq 1$. The trend that ρ decreases with Z and the decay is faster for larger strains clearly indicates the decorrelation effects of the actual strain on the pre- and post-compression waveforms.

The variance of the strain estimate $\sigma^2(\hat{s})_{\mathrm{ZZLB},\rho}$ is plotted as a function of the window length Z in Fig. 4 for the same strain values ($s = 0\%$, 0.5%, 1%, 2%, and 5%) used in Fig. 3. For $s = 0$, $\sigma^2(\hat{s})_{\mathrm{ZZLB},\rho}$ decreases with Z and the result converges to the asymptote proportional to Z^{-3} (since the variance is bounded by the CRLB in this region) because $\sigma^2(\hat{d})_{\mathrm{CLRB},\rho} \propto Z^{-1}$ at large Z. For $s \neq 0$, however, the variance is larger and does not decay as fast with Z. The strain induced effects on the variance are observed as a rapid rise after a characteristic window length depending on the strain. The variance of the strain estimate is minimum at a characteristic time-bandwidth product that depends on the strain. Because the bandwidth is maintained constant, the strain estimation variance is minimum at this particular window length, which is referred to as the optimal window length in this paper.

The dependence of the elastographic SNR_e on the window length Z is depicted in Fig. 5 for strains: $s = 0.5\%$, 1%, 2%, and 5%. Note that SNR_e, which is inversely proportional to $\sigma(\hat{s})_{\mathrm{ZZLB},\rho}$ according to (4), is calculated by setting the mean strain equal to the actual strain, i.e., $m_s = s$, because the displacement estimator based on the cross-correlation peak is unbiased [15]. The curves exhibit distinct peaks for each strain with the corresponding optimal window lengths maximizing the elastographic SNR_e. Large strains shift the peak in the SNR_e curve to smaller window lengths while reducing the peak value of the SNR_e. Analysis of the results from Fig. 5 resulted in the following empirical formula for the optimal window length:

$$T_{\mathrm{opt}} \cong \frac{3B}{2sf_0^2} \tag{17}$$

where B is the bandwidth and f_0 is the center frequency of the ultrasonic pulse. Fig. 6 presents plots of (17) for two different transducer center frequencies along with the corresponding theoretical results. Observe from Fig. 6 that this empirical relationship characterizes the variation in the optimal window length with strain.

The multiresolution strain filter characterizes the sensitivity and dynamic range of the elastograms from the signal and the noise properties of the elastograms. The strain filters for four different window lengths, $Z = 0.5$, 1, 3, and 5 mm are illustrated in Fig. 7. The results clearly show the tradeoff between the improvement in both elastographic sensitivity and dynamic range with Z versus the reduction in elastographic resolution. Small windows perform better for the elastographic imaging of regions with large strains at the expense of increased strain noise. The sharp decline observed at very high strains are due to the uncertainties in determining the location of correlation peak as discussed previously in [4].

Fig. 8 presents a three-dimensional plot of the strain filter with resolution, tissue strain, and elastographic SNR_e plotted along the three axes. Note that the sensitivity reduces with an improvement in the resolution as seen by the movement of the strain filter toward higher tissue strains. The strain filter also becomes shorter, with a sharp decline in the SNR_e observed at very high resolutions as illustrated in Fig. 8. Plotting the strain filters in this manner allows the visualization of the entire range of tissue strains observable in the elastogram at different resolutions.

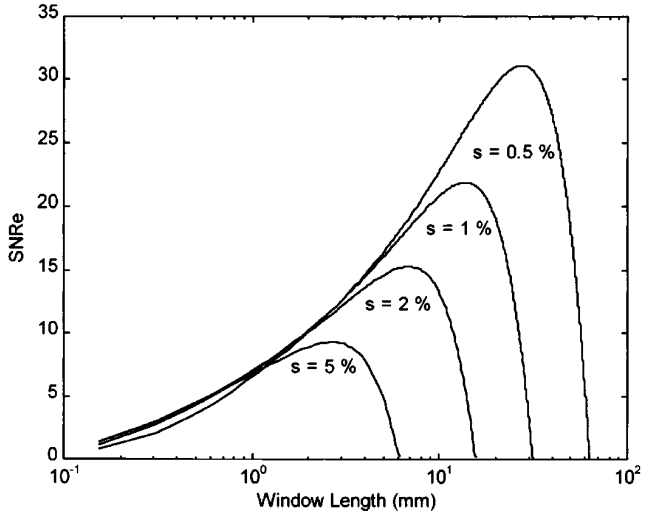

Fig. 5. Elastographic SNR_e plotted as a function of the window length, using the CRLB on the variance of the strain estimator. Note that the SNR_e is maximum for strain values at the optimal window length obtained from Fig. 1. The SNR_e estimates were obtained using the following parameters: $L_h = L_f = 0.1$ mm, $k_0 = k_f = 20.4$ mm^{-1}.

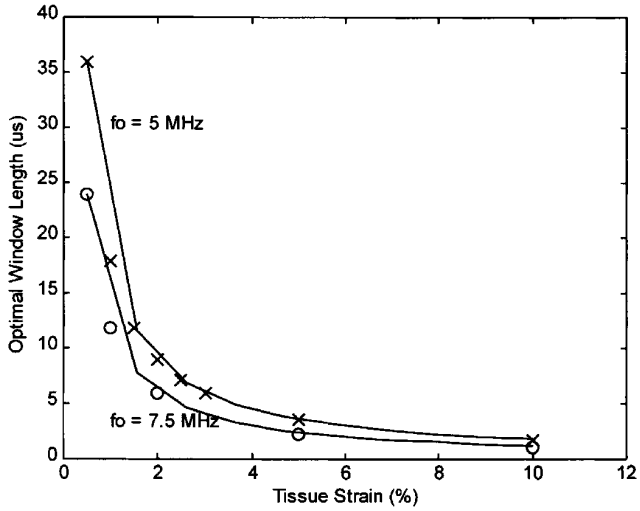

Fig. 6. The optimal window lengths plotted as a function of their respective strain values with center frequencies of 5 MHz (x x x) and 7.5 MHz (o o o) and a 60% bandwidth, respectively. The solid line denotes the empirical plot obtained using (17) for the 5 MHz and 7.5 MHz transducer, respectively. Note the close correspondance between the empirical and theoretical results. The optimal window length increases rapidly with a decrease in tissue strain.

In the next two sections, we test the performance of the multiresolution strain filter with numerical simulations and experimental measurements.

V. Simulation Results

In this section, we use one-dimensional Monte-Carlo simulations in MATLAB to corroborate the theoretical results presented in the previous section.

A. Method

The A-scan RF echo signals were simulated using a Gaussian PSF with 7.5 MHz center frequency and 50% bandwidth ($L_h = 0.06$ mm) and sampled at 48 MHz. The speed of sound in tissue was assumed to be constant at 1540 m/s. The scattering function consists of uniformly distributed high density point scatterers (40 scatterers/resolution cell) satisfying the requirement of fully developed speckle. The PSF is convolved with the scattering function to obtain the pre-compression A-scans.

The displacement of the point scatterers in a uniform medium due to the static compression was derived by Céspedes [3]. The applied stress is assumed to propagate uniformly so that the displacement of each scatterer can be written as a function of the applied strain and the position of the surrounding scatterers. Considering an equivalent one-dimensional spring system [3], the displacement (d_i) of the ith scatterer due to an applied displacement of Δy is given by:

$$d_i = \frac{\Delta y l_i}{L}, \tag{18}$$

where L is the length of the tissue medium, and l_i is the location of the ith scatterer. The post-compression A-scan is obtained by convolving the PSF with the compressed point scatterers. A total of 25 independent scattering functions and the corresponding pre- and post-compression signal pairs are realized. The strain estimates are then computed from these signal pairs using different window lengths. The value of SNR_e is calculated from the mean m_s and the standard deviation σ_s of the strain estimates.

The above process is repeated for two strains $s = 1\%$ and 2%.

B. Results

The variation of SNR_e with the window length is plotted for the two strains $s = 1\%$ and 2% in Fig. 9. The graphs with the error-bars and symbols denote the simulation results: "x" for $s = 1\%$ and "o" for $s = 2\%$ and the solid line represent the theoretical predictions of the multiresolution strain filter obtained for $L_f = 0$ in (13) and (14). The graphs of both the theoretical and simulation results illustrate similar features of increasing with Z and reaching a maxima at a characteristic Z value and decaying with further increase in Z. The theory overpredicts the SNR_e as expected because it describes the upper bound on the performance of the strain estimator. In addition, the simulation uses a Gaussian shaped PSF and the strain filter is obtained using a flat spectrum. The multiresolution strain filter, therefore, can be used to guide the selection of the optimal window length and consequently the optimal resolution.

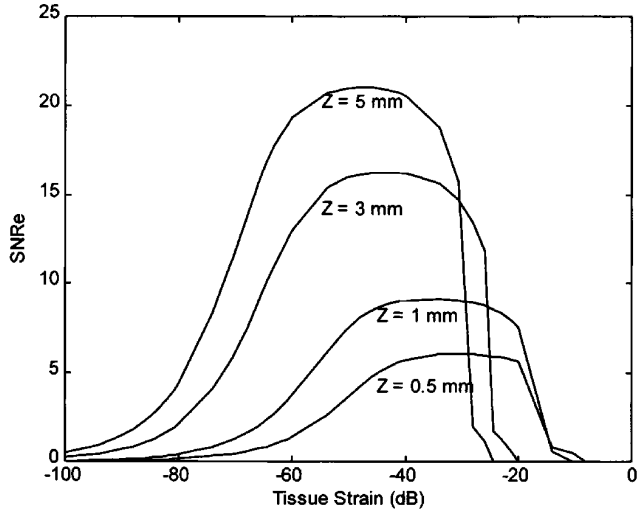

Fig. 7. A group of four strain filters, showing the distinct regions of strain estimation. These strain filters correspond to resolutions of 0.5 mm, 1 mm, 2 mm, and 5 mm, respectively. The strain filters were obtained using the following parameters: $L_h = L_f = 0.1$ mm, $k_0 = k_f = 20.4$ mm^{-1}. Note the improvement in the sensitivity with a decrease in elastographic resolution.

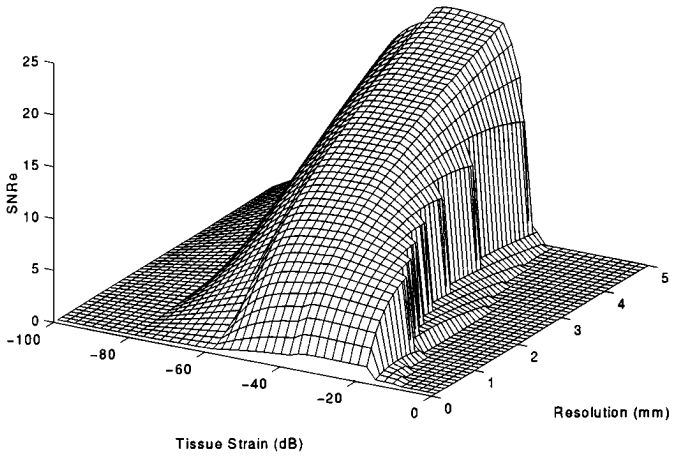

Fig. 8. The multiresolution strain filter in elastography. Tissue strain in dB is plotted along the x-axis, resolution along the y-axis, and SNR_e along the z-axis. Note the variation in the shape of the strain filter, which shifts toward lower strains with a decrease in the resolution. The strain filters were obtained using the following parameters: $L_h = L_f = 0.1$ mm, $k_0 = k_f = 20.4$ mm^{-1}.

VI. Experimental Results

In this section, experimental results are presented to support the use of the multiresolution strain filter as a quantitative measure for evaluating the elastographic imaging systems. The elastography system consists of a Diasonics Spectra II scanner (Diasonics Inc., Santa Clara, CA) with a 7.5 MHz linear array, a digitizer (LeCroy Corp., Spring Valley, NY) operating at 48 MHz, a motion control system, and a compression device. A personal computer controls the operation of the entire system.

A gelatin phantom that contains graphite flakes for speckle scattering and an inclusion that is positioned at the center and three times stiffer than the background is used during the measurement [21]. A large compressor was used for uniform compression producing 1% applied strain, and ultrasonic RF A-lines are acquired before and after the compression. The sonogram obtained from the pre-compression A-lines is shown in Fig. 10(a); the elastogram obtained using a single 3 mm window is illustrated in Fig. 10(b). Figs. 10(c–e) represent elastograms of the phantom obtained using multiresolution elastography. Note that the inclusion is barely visible in the sonogram due to similar acoustic backscattering in both the inclusion and background. However, the inclusion can be clearly seen in the elastograms.

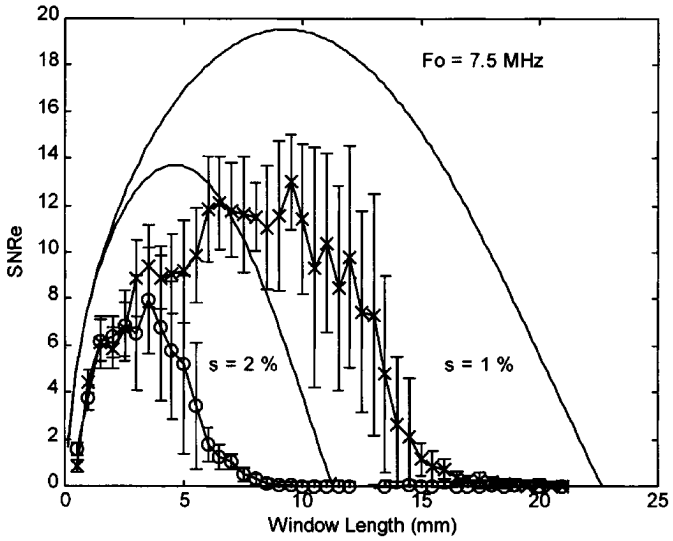

Fig. 9. Simulation and theoretical results that illustrate the variation in SNR_e with window length. Note the similar location of the optimal window length in both the theoretical and simulation results. Both the theoretical and simulation results were obtained using the following parameters: $L_h = 0.06$ mm (50% bandwidth) $L_f = 0$, $k_0 = 30.6$ mm^{-1}.

Multiresolution analysis is carried out by processing the RF pre- and post-compression data with different window lengths. The strains with the highest SNR_e are selected to generate the composite elastogram. The elastographic SNR_e at each pixel in the elastogram is computed from the ratio of the measured strain value to its corresponding standard deviation [obtained by substituting the value of the correlation coefficient from the windowed pre- and post-compression waveforms into (6)]. Elastograms and the corresponding SNR_e mappings are obtained at each window length. The tissue strain at each pixel corresponding to the highest value of SNR_e within the range of window lengths is selected as the strain estimate in the composite elastogram.[3] The smallest window length was fixed at 1 mm, and subsequent multiresolution processing was performed with additional 0.5 mm increments on the win-

[3]The elastograms in this section are processed without temporal stretching. For nonuniform targets, an adaptive stretching technique [22] has to be used to improve the elastogram parameters.

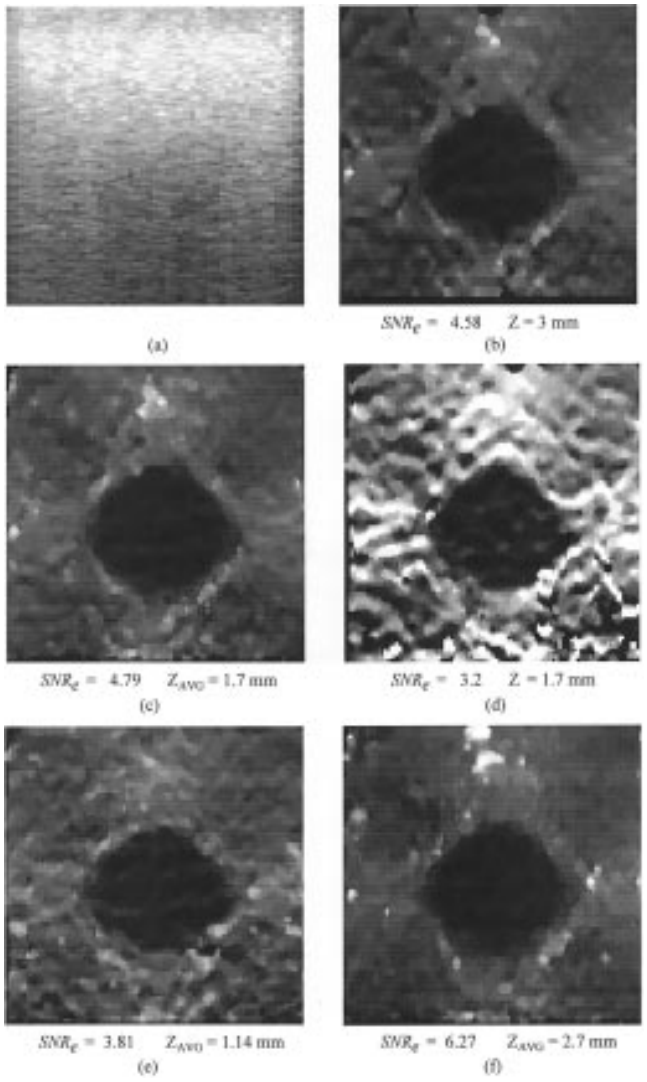

Fig. 10. Sonogram (a) and elastograms (d–e), with a 1% total compression, for a phantom with an inclusion that is three times stiffer than the background. The sonogram was obtained using a 7.5 MHz (k_0 = 30.6 mm^{-1}) linear array with a 50% bandwidth. The elastogram in (b) was obtained using a single 3 mm window, while (c) represents the elastogram obtained using multiresolution elastography with the largest window length used = 3 mm. Compare the multiresolution elastogram in (c) with the elastogram in (d) which was obtained using z = 1.7 mm. The composite elastograms shown in (e) and (f) were obtained using multiresolution elastography with the largest window length used = 2 mm and 4 mm, respectively.

dow length. The composite elastograms are presented in Figs. 10(c, e, f).

A comparison of the elastograms obtained using multiresolution processing as opposed to the traditional method of using a single window length is illustrated in Figs. 10(b–d). Quantitative values of the elastographic SNR_e (computed in a small uniform region near the top left corner of the elastogram) and the average resolution (Z_{AVG}) in the elastogram are also presented in Figs. 10(b–f). Z_{AVG} is estimated by computing a weighted sum of the window length times the percentage of the strain estimates computed using that window. Note that, although

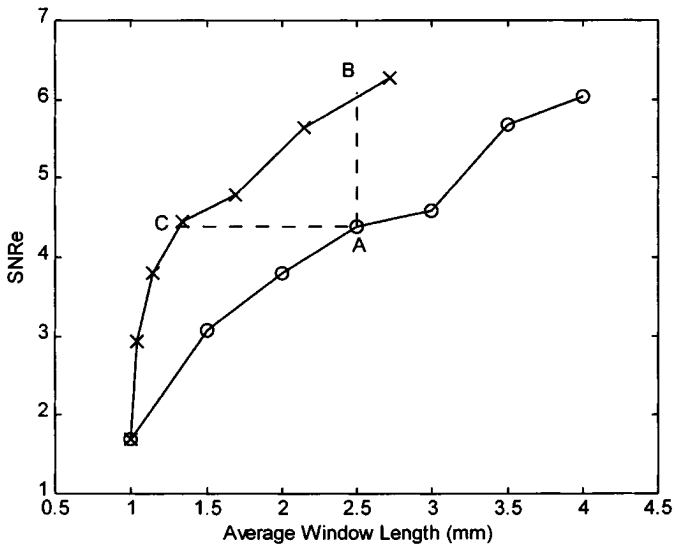

Fig. 11. Comparison of the elastogram parameters obtained using multiresolution (x-x-x) and single resolution (o-o-o) elastography. The elastographic SNR_e and the average resolution were computed for the elastograms generated in Fig. 10.

the SNR_e values for both these elastograms are in the same range, a significant improvement in the average resolution is observed in the multiresolution elastogram. For a realistic comparison of the SNR_e improvement, the multiresolution elastogram in Fig. 10(c) should be compared to the single resolution elastogram obtained using Z = 1.7 mm [Fig. 10(d)]. The selection of the strains with the highest SNR_e in multiresolution elastography significantly reduces the bias artifacts [3] that can be observed clearly in Fig. 10(d). These bias artifacts increase with a decrease in the window length used to obtain the elastogram. The elastographic SNR_e, however, is not significantly affected by the bias artifacts because the first order statistics used to compute the SNR_e are virtually unchanged. The evolution of the elastographic SNR_e with the average resolution parameter is illustrated in Fig. 11, for both multiresolution (denoted by 'x') and single resolution elastography (denoted by 'o'). Observe from Fig. 11, that comparing the two techniques at the same average resolution (2.5 mm) produces a significant improvement in the SNR_e (denoted in Fig. 11 as the increase from A to B). In addition, a comparison of the elastograms at the same elastographic SNR_e, indicates the improvement in the average resolution parameter (denoted by the improvement in the average resolution form A to C).

The enhancement of the elastogram image parameters can be described in terms of the strain filter formulation as illustrated in Fig. 12. In addition to improvements in the SNR_e and Z_{AVG}, we also obtain an increase in the dynamic range using multiresolution elastography. Comparing the strain filters for the above result, we obtain DR_e = BD for the elastogram using the single window when compared to DR_e = BE with multiresolution processing for a 3 mm resolution. The elastogram in Fig. 10(e) was obtained at a 2 mm resolution (using three elastograms or 3 mul-

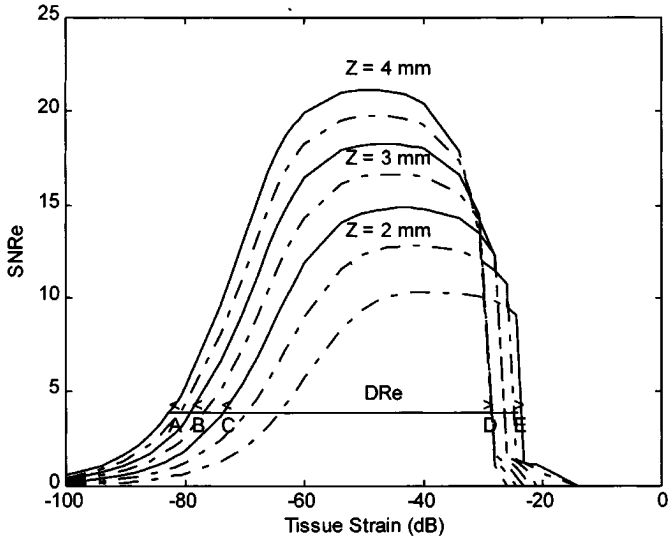

Fig. 12. The corresponding multiresolution strain filters for the elastograms shown in Fig. 10. The strain filters were obtained using the following parameters: $L_h = L_f = 0.06$ mm, $k_0 = k_f = 30.6$ mm^{-1}.

tiresolution steps to generate the composite elastogram), and Fig. 10(f) represents the case with a 4 mm resolution (using seven elastograms). Note the improvement in the composite elastograms obtained with an increase in multiresolution processing as observed in Figs. 10(c, e, f). Observe from the corresponding strain filters in Fig. 12 that DR_e = CE for Fig. 10(e) (using three elastograms), DR_e = BE for Fig. 10(c) (using five elastograms) and DR_e = AE for Fig. 10(f) (using seven elastograms).

Multiresolution elastography, as illustrated in Figs. 10(c, e, f) improves both the elastographic SNR_e and dynamic range by proper selection of the strain estimates from the individual elastograms. The elastograms improve with an increase in the multiresolution steps as indicated in Fig. 10. However, the improvement in the elastogram parameters does not increase linearly with the number of multiresolution steps as observed in the improvements in the elastogram from Figs. 10(e) to (c) (increase in the dynamic range by BC = 6 dB, and maximum SNR_e value by 3), when compared to Figs. 10(c) and (f) (increase in the dynamic range by AB = 4 dB, and maximum SNR_e value by 2) for the same computation time. In addition, the average resolution in the multiresolution elastogram also reduces with an increase in the multiresolution steps.

VII. Discussion and Conclusions

Multiresolution elastography is presented in this paper as a method of maximizing the overall SNR_e in the elastogram, in addition to increasing the dynamic range of strains estimated and enhancing the average resolution. The importance of the strain filter formulation is its ability to adaptively guide the strain estimation process. Although the strain filter is theoretically formulated for the cross-correlation based strain estimation algorithm, this concept is valid for any elastographic technique that uses an unbiased displacement estimator, because the formulation is based on well known bounds.

The theoretical formulation of the strain filter now includes the limitations imposed by the use of the finite cross-correlation window to estimate tissue strain. The window length parameter contributes to the strain filter formulation in two ways: first, through the expression for the CRLB (modified for partially correlated signals), and second, through the dependence of the effective correlation coefficient on the window length (14). The strain estimation variance used in the strain filter model is now a function of both the tissue strain and the window length. The acoustic signal model used to derive the correlation coefficient is one-dimensional and, therefore, does not include the effects of additional derating due to lateral and elevational decorrelation. However, the multiresolution strain filter with this simple model still provides valuable insights into the elastogram parameters obtainable at different resolutions.

The presence of an optimal window length where the increased information in the RF signal is surpassed by the signal decorrelation due to tissue strain and the movement of tissue scatterers within the finite window is illustrated in this paper. The theoretical analysis for the presence of the optimal window length (using the CRLB on the variance of the strain estimator modified for partially correlated signals) is corroborated by the simulation results. The composite elastograms obtained using multiresolution elastography [Figs. 10(c, e, f)], illustrate the improvement in the elastogram parameters obtained using a single set of RF pre- and post-compression data. Multiresolution elastography provides minimum variance strain estimates. The corresponding multiresolution strain filter allows a clear visualization of the range of strains observable in the elastogram.

The multiresolution strain filters illustrated in this paper are obtained at a fixed depth in tissue (at the focus or in the far field of the ultrasonic beam) and under the assumption that lateral and elevational decorrelation effects can be ignored. However, the characteristics of the strain filter also depend on lateral and elevational position and the depth in tissue [5], [6]. A family of strain filters can be obtained at different depths or at different lateral and elevational positions, thereby incorporating another dimension to the strain filter concept [5], [6].

Acknowledgment

The elastographic phantom used in this paper was supplied courtesy of Dr. Timothy Hall.

Appendix

A. Definitions

Composite signal-to-noise ratio: The composite signal-to-noise ratio (SNR_C) is a combination of the sonographic

noise level (SNR_S) and a noise component due to signal decorrelation, and is given by [12]:

$$\frac{1}{\mathrm{SNR}_C} = \frac{1}{\mathrm{SNR}_S} + \frac{1}{\mathrm{SNR}_\rho} \tag{A-1}$$

where $\mathrm{SNR}_\rho = \rho/1-\rho$ converts the correlation coefficient to an SNR measure. The above relationship enables the use of SNR_C in CRLB expressions in the literature that involve signal decorrelation. This allows incorporation of signal processing algorithms and decorrelation effects due to lateral motion, attenuation, etc. into the strain filter. Note that SNR_C will always be bounded by the smallest value of either SNR_S or SNR_ρ.

Strain dynamic range: The range of strains that can be depicted in an elastogram at high SNR_e determines the dynamic range of the strain filter, which is defined as:

$$\mathrm{DR}_e|_{\mathrm{SNR}_e,\mathrm{ref}} = 20\log_{10}\left[\frac{s_{\max}}{s_{\min}}\right] \tag{A-2}$$

where $s_{\max}$ is the maximum strain and $s_{\min}$ is the minimum strain at a specified $\mathrm{SNR}_{e,\mathrm{ref}}$ level in the strain filter. In this paper we have chosen the specified $\mathrm{SNR}_e = 4$ (Fig. 12).

Strain sensitivity: Strain sensitivity is defined as the smallest value of the strain in the elastogram depicted at a specified value of the SNR_e. The quantity $s_{\min}$ also defines the sensitivity of the strain filter.

$$\text{Sensitivity} = s_{\min}|_{\mathrm{SNR}_e,\mathrm{ref}} \tag{A-3}$$

Equivalent square bandwidth of a Gaussian spectrum: A reasonable approximation using a rectangular spectrum centered at the Gaussian center frequency with the same mean square amplitude value as the Gaussian spectrum is obtained. The equivalent noise spectral bandwidth [23, p. 141] is defined by:

$$B = \frac{\int_0^\infty |P(k)|^2\,dk}{|P(k)|^2_{\max}} = \frac{\frac{1}{4\pi}\int_{-\infty}^{\infty}|P(k)|^2\,dk}{|P(k)|^2_{\max}} = \frac{1}{2\sqrt{\pi}L_h} \tag{A-4}$$

where B is the bandwidth of a rectangular spectrum with the same total power and peak amplitude as the Gaussian pulse spectrum $P(k)$.

B. Threshold Values for the ZZLB

The threshold values used in (5) are defined as follows:

$$\begin{aligned}\eta &= \frac{6}{\pi^2}\left(\frac{f_0}{B}\right)^2\left[\varphi^{-1}\left(\frac{B^2}{24f_0^2}\right)\right]^2\\ \vartheta &= \frac{2.76}{\pi^2}\left(\frac{f_0}{B}\right)^2\\ \delta &= \zeta/2\\ \gamma &\approx 0.46\end{aligned} \tag{B-1}$$

where $f_0 = 1/\lambda_0$ is the center frequency, B is the equivalent rectangular spectral bandwidth, $\varphi^{-1}(y)$ is the inverse of $\varphi(y) = \frac{1}{\sqrt{2\pi}}\int_y^\infty e^{-\mu^2/2}d\mu$, and $(\zeta/2)\varphi(\sqrt{\zeta/2}) = (12/BcsZ)^2$, which has two solutions. The larger value of ζ is used to compute the threshold. When $\eta < (2BZ/c)\mathrm{SNR}_C$, the ZZLB coincides with the CRLB, which is the ambiguity-free region. If $\delta < (2BZ/c)\mathrm{SNR}_c < \vartheta$, the ZZLB coincides with the Barankin bound, where phase ambiguities increase the displacement variance. Finally when $(2BZ/c)\mathrm{SNR}_c < \gamma$, the lower bound is characterized by the constant variance level of $(sZ)^2/6Z\Delta z$, which corresponds to the variance of a random variable uniformly distributed between $[-sZ/2, sZ/2]$.

References

[1] J. Ophir, E. I. Céspedes, H. Ponnekanti, Y. Yazdi, and X. Li, "Elastography: a quantitative method for imaging the elasticity of biological tissues," *Ultrason. Imaging*, vol. 13, pp. 111–134, 1991.

[2] J. Ophir, F. Kallel, T. Varghese, M. Bertrand, I. Céspedes, and H. Ponnekanti, "Elastography: a systems approach," *Int. J. Imaging Syst. Technol.*, vol. 8, pp. 89–103, 1997.

[3] E. I. Céspedes, "Elastography: imaging of biological tissue elasticity," Ph.D. Dissertation, University of Houston, Houston, TX, 1993.

[4] T. Varghese and J. Ophir, "A theoretical framework for performance characterization of elastography: the strain filter," *IEEE Trans. Ultrason., Ferroelect., Freq. Contr.*, vol. 44, no. 1, pp. 164–172, 1997.

[5] T. Varghese and J. Ophir, "The nonstationary strain filter in elastography. Part I. Frequency dependent attenuation," *Ultrason. Med. Biol.*, vol. 23, no. 9, pp. 1343–1353, 1997.

[6] F. Kallel, T. Varghese, J. Ophir, and M. Bilgen, "The nonstationary strain filter in elastography. Part II. Lateral and elevational decorrelation," *Ultrason. Med. Biol.*, vol. 23, no. 9, pp. 1354–1367, 1997.

[7] M. O'Donnell, A. R. Skovoroda, and B. M. Shapo, "Measurement of arterial wall motion using Fourier based speckle tracking algorithms," *Proc. IEEE Ultrason. Symp.*, 1991, pp. 1101–1104.

[8] T. Varghese, J. Ophir, and E. I. Céspedes, "Noise reduction in elastography using temporal stretching with multicompression averaging," *Ultrason. Med. Biol.*, vol. 22, no. 8, pp. 1043–1052, 1996.

[9] E. E. Konofagou, J. Ophir, F. Kallel, and T. Varghese, "Elastographic dynamic range expansion using variable applied strains," *Ultrason. Imaging*, vol. 19, no. 1, 1997.

[10] T. Varghese and J. Ophir, "Characterization of elastographic noise using the envelope of echo signals," submitted for publication.

[11] E. I. Céspedes, M. F. Insana, and J. Ophir, "Theoretical bounds on strain estimation in Elastography," *IEEE Trans. Ultrason., Ferroelect., Freq. Contr.*, vol. 42, pp. 969–972, 1995.

[12] E. Weinstein and A. Weiss, "Fundamental limitations in passive time delay estimation. Part II: Wide-band systems," *IEEE Trans. Acoust., Speech, Signal Processing*, vol. ASSP-31, pp. 1064–1078, 1984.

[13] F. W. Walker and E. G. Trahey, "A fundamental limit on delay estimation using partially correlated speckle signals," *IEEE Trans. Ultrason., Ferroelect., Freq. Contr.*, vol. 42, pp. 301–308, 1995.

[14] A. H. Quazi, "An overview of the time delay estimate in active and passive systems for target localization," *IEEE Trans. Acoust., Speech, Signal Processing*, vol. ASSP-29, pp. 527–533, 1981.

[15] C. H. Knapp and G. C. Carter, "The generalized correlation method for estimation of time delay," *IEEE Trans. Acoust., Speech, Signal Processing*, vol. ASSP-24, pp. 320–327, 1976.

[16] F. W. Walker and E. G. Trahey, "A fundamental limit on the accuracy of speckle signal alignment," *Proc. IEEE Ultrason. Symp.*, 1994.
[17] M. Bilgen and M. F. Insana, "Error analysis in acoustic elastography: II Strain estimation and SNR analysis," *J. Acoust. Soc. Amer.*, vol. 101, no. 2, pp. 1147–1154, 1997.
[18] M. Bilgen and M. F. Insana, "Deformation models and correlation analysis in elastography," *J. Acoust. Soc. Amer.*, vol. 99, pp. 3212–3224, 1996.
[19] F. L. Lizzi, M. Ostromogilsky, E. J. Feleppa, M. C. Rorke, and M. Yaremko, "Relationship of ultrasonic spectral parameters to features of tissue microstructure," *IEEE Trans. Ultrason., Ferroelect., Freq. Contr.*, vol. 34, pp. 319–329, 1987.
[20] M. F. Insana, R. F. Wagner, D. G. Brown, and T. J. Hall, "Describing small scale structure in random media using pulse-echo ultrasound," *J. Acoust. Soc. Amer.*, vol. 87, pp. 179–192, 1990.
[21] T. J. Hall, M. F. Insana, and M. Bilgen, "Developing phantoms for elastography," (Abstract) in *Proc. 21st Int. Symp. Ultrason. Imaging Tissue Characterization*, June 3–5, 1996.
[22] S. K. Alam and J. Ophir, "An adaptive strain estimator for elastography," submitted for publication.
[23] J. S. Bendat and A. C. Piersol, *Random Data: Analysis and Measurement*, 2nd Ed. New York: Wiley, 1986.

Tomy Varghese (S'92–M'96) received the B.E. degree in instrumentation technology from the University of Mysore, India, in 1988, and the M.S. and Ph.D. in electrical engineering from the University of Kentucky, Lexington, KY, in 1992 and 1995, respectively.

From 1988 to 1990 he was employed as an engineer in Wipro Information Technology Ltd., India. He is currently a postdoctoral research associate at the Ultrasonics Laboratory, Department of Radiology, The University of Texas Medical School, Houston.

His current research interests include detection and estimation theory, statistical pattern recognition, tissue characterization using ultrasound, and signal and image processing applications in medical imaging. Dr. Varghese is a member of the IEEE and Eta Kappa Nu.

Mehmet Bilgen (M'97) was born in Nazilli, Turkey on December 10, 1965. He received the B.S. degree (summa cum laude) in Electrical and Electronics Engineering from Middle East Technical University Gaziantep Campus (currently Gaziantep University), Gaziantep, Turkey, in 1987 and the M.S. and Ph.D. degrees in Electrical and Computer Engineering and Biomedical Engineering from Iowa State University, Ames, Iowa in 1989 and 1993, respectively.

From 1987 to 1988 he was a R&D engineer at Aselsan Inc. while continuing his graduate study at Middle East Technical University, Ankara, Turkey. He was a postdoctorate researcher at Center for Nondestructive Evaluation, Ames, Iowa, where he worked in inspections of materials with rough surfaces and underground pipes. He is currently a postdoctorate researcher in The Department of Radiology at University of Kansas Medical Center. His research interests are elastography, tissue characterization, nondestuctive evaluation, wave propagation in inhomogeneous media, and signal processing.

Dr. Bilgen is a three-year scholarship recipient from The Scientific and Technical Research Council of Turkey.

Jonathan Ophir (M'97) received his B.S.E.E. (Summa Cum Laude), M.S.E.E., and Doctor of Engineering degrees from the University of Kansas, Lawrence, KS, in 1971, 1973, and 1977, respectively. His doctoral dissertation describes an early implementation of digital scan conversion techniques for diagnostic ultrasound. During 1976 and 1977 he worked as a project engineer for Philips Ultrasound Inc., where he developed a commercial version of their first digital scan converter. He then spent 3 years as an assistant professor of radiology at the University of Kansas Medical School in Kansas City, KS, where he was involved in the development of prototype sonographic contrast agents, ultrasound phantoms, and instrumentation for ultrasonic tissue characterization. From 1980 until the present time, he has been with the University of Texas Medical School at Houston, where he is currently Professor of Radiology. He is also Adjunct Professor of Electrical Engineering at the University of Houston. His current field of interest is elastography, the imaging of the elastic properties of soft tissues.

Dr. Ophir has contributed more than 85 paper to peer reviewed scientific journals and holds 15 US and foreign patents. He is a Fellow of the American Institute of Ultrasound in Medicine, past Chairman of their Standards Committee, and past Member of the Board of Governors. He is a member of the Editorial Board of *Ultrasound in Medicine and Biology*, and is Associate Editor of *Ultrasonic Imaging*. In 1992 he received the Terrance Matzuk Award from the American Institute of Ultrasound in Medicine, and in 1995 he was recognized as Inventor of the Year by the Mayor of the City of Houston, TX. In 1995 he also recieved an honorary commission as an Admiral in the Texas Navy by Governor George W. Bush.